COBEM 2021 26th International Congress of Mechanical Engineering
November 22-26, 2021, Virtual Congress, Brazil
ABCM Associação Brasileira de Engenharia e Ciências Mecânicas

# COB-2021-0197
# LOW-FREQUENCY SOUND ABSORPTION WITH BANDWIDTH EXPANDED BY SYMMETRIC LABYRINTHINE ACOUSTIC METAMATERIAL

**Gildean do N. Almeida**
**Erasmo F. Vergara**
**Leandro R. Barbosa**
**Robson Z. Mikulski**
Federal University of Santa Catarina, R. Eng. Agronômica Andrei C. Ferreira, s/n-Trindade, Florianópolis-SC, Brasil, 88040 − 900.
gildean_fsa@hotmail.com; e.f.vergara@ufsc.br

***Abstract.*** *Due to the weak dissipation of traditional materials in the region of low frequencies ($\leq$ 600 Hz), the sound absorption in this region through the acoustic metamaterials (AMM) is of great interest to noise control engineering. In this study, we analytically, numerically and experimentally investigated an AMM composed of a rigid panel containing a micro-perforation of the micro slit type coupled to a multi-cavity of coiled-up channels. The strategy of symmetrical channels together with visco-thermal losses determines the position of the peak of sound absorption and allows greater control of sound energy. The additive manufacturing technology was used to manufacture the absorber, which was evaluated in the impedance tube technical apparatus for sound waves of normal incidence. Sound absorption of 97% at 242 Hz with a relative bandwidth of 65% was obtained experimentally and showed good agreement with the theoretical and numerical models. This agreement is mainly due to the high dissipation of sound energy in the micro slit region. Therefore, this study reveals the possibility of designing rigid, lightweight structures, and with sub-wavelength dimensions ($\lambda/32$), since these structures are of great interest in the fields of engineering acoustics and materials.*

***Keywords:*** *Acoustic metamaterial, Low-frequency sound absorption, Additive manufacturing, Sub-wavelength, Visco-thermal effects*

## 1. INTRODUCTION

For decades, the control of the sound energy associated with low frequencies through materials with sub-wavelength dimensions has been a challenge for the scientific community. Although traditional porous materials and micro-perforated panels are efficient in controlling this energy, these materials require large scales to be operative in this frequency region (Carvalho de Sousa *et al.*, 2021; Almeida *et al.*, 2021a). Thus, with the advent of acoustic metamaterials (AMM), new perspectives have emerged for the control of this energy through structures presenting sub-wavelength scales. In fact, this perspective is mainly through the geometric arrangement of these structures.

Due to their wide applicability, acoustic metamaterials also stand out as an alternative in terms of manipulation, mitigation and control of sound energy. By acoustic metamaterials presupposes periodic structures that have unique properties and behaviors for large wavelengths (Gan, 2018). This unique behavior of AMMs occurs mainly due to the strong coupling of its surface impedance with that of the medium, thus allowing the sound wave to pass efficiently into its interior without any reflection (Almeida *et al.*, 2021c; Li *et al.*, 2016). Furthermore, these absorbers present a high capacity for converting sound energy into thermal or viscous energy. In this sense, different structures have been proposed, including those based on Helmholtz resonators (Zhao *et al.*, 2017; Wu *et al.*, 2016; Tang *et al.*, 2017b), those based on resonant membranes (Leblanc and Lavie, 2017; Langfeldt *et al.*, 2017) as well as which are based on Fabry-Pérot (FP) type channels simple (Long *et al.*, 2019; Cai *et al.*, 2014; Almeida *et al.*, 2021c) or symmetrical (Almeida *et al.*, 2021b).

In this work, based on the concept of symmetrical coiled-up channels and visco-thermal losses, we discuss analytically, numerically and experimentally the behavior of an AMM composed of a rigid panel with a slit type micro-perforation coupled to a multi-cavity of spaces that resembles a symmetric labyrinth. It is demonstrated that the increase in symmetrical coiled-up spaces and the influence of visco-thermal losses determine the frequency of the sound absorption peak and allow a greater control of sound energy. It is verified that viscous energy dissipation predominates over thermal dissipation in the AMM. Moreover, a sound absorption of 97% at 242 Hz with a bandwidth of 65% was obtained in the experiments and is in good agreement with the theoretical and numerical methods.

This article is organized in five sections: the general aspects of the AMM structure, its respective geometric parameters and the theoretical method are described in Section 2. A brief presentation of numerical analysis using the finite element

method (FEM) is described in Section 3. Theoretical, numerical and experimental results and a detailed discussion are presented in Section 4. Finally, the conclusion of the work is presented in Section 5.

## 2. MATERIALS AND METHODS

### 2.1 The structure of the AMM unit

The structure of an absorber unit cell containing five coiled-up channels and a top view on the $xy$ plane are illustrated in Figure 1 a) and b), respectively. It can be seen that the model cell has width $m$, height $L$ and thickness $h$, the rigid front panel has thickness $t$, and in the geometric center of the plane $yz$ is located the micro slit of width $d_f$ on axis $y$ and height $L_f$ on axis $z$. The cross section of the symmetrical coiled-up channels has height $W$ and width $a$. The walls that form the coiled-up channels presents thickness $b$ and, behind the structure, a rigid panel prevents the leakage of sound waves.

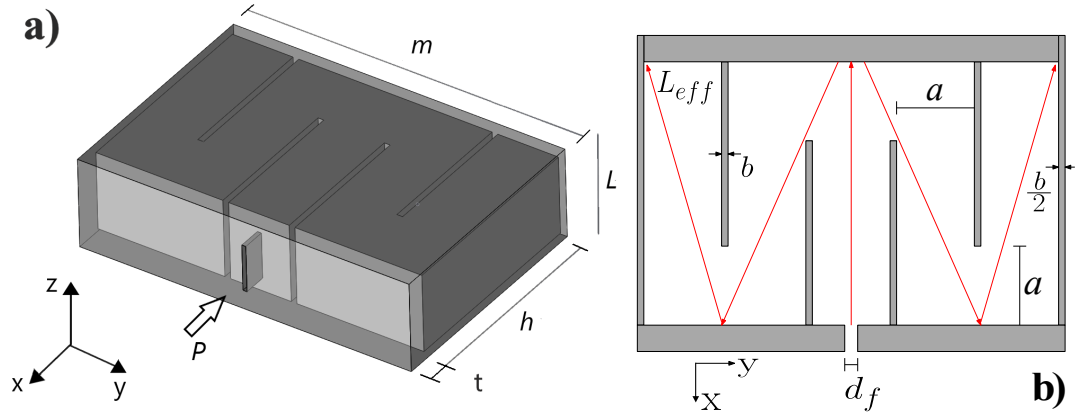


Figure 1. Structure of acoustic metamaterial with double coiled-up channels. a) Unitary cell and b) section view of a unit cell in the $xy$ plane.

### 2.2 The sound absorption coefficient of the AMM unit and theoretical method

Considering that a normal plane wave of amplitude $P$ is incident on the AMM panel, the sound absorption coefficient of the rigidly supported absorber can be obtained from its surface impedance $Z_S$, which is obtained by Eq. 1

$$\alpha = 1 - \left| \frac{Z_S/Z_0 - 1}{Z_S/Z_0 + 1} \right|^2, \tag{1}$$

with $Z_0 = \rho_0 c_0$ being the characteristic air impedance and $\rho_0 = 1.21$ kg·m$^{-3}$ and $c_0 = 343$ m·s$^{-1}$ being the density and speed of sound in the air, respectively. Note that the $Z_S$ is a complex quantity, so when $\mathrm{Re}(Z_S) = 1$ and $\mathrm{Im}(Z_S) = 0$, we have the condition of strong coupling between the surface impedance of the absorber and the air impedance. The surface impedance is obtained by associating in parallel the total impedance $Z_{T_i}$ of each coiled-up channel (Almeida *et al.*, 2021b), that is,

$$Z_S = \frac{Z_{T_1} \times Z_{T_2}}{Z_{T_1} + Z_{T_2}} = \frac{(Z_p + \xi Z_{e_1}) \times (Z_p + \xi Z_{e_2})}{2Z_p + \xi Z_{e_1} + \xi Z_{e_2}}, \tag{2}$$

where $Z_p$ and $Z_{e_i}$ are the front panel impedance and the acoustic impedance of the coiled-up channel, respectively, with $i = 1, 2$ being the coiled-up channel under analysis and $\xi = S_0/S_i$ is the area modifying factor that maintains the conservation of the volume velocity flow. Here $S_0 = mL$ and $S_i = aW$ represent the areas of the unit cell and the cross section of the coiled-up channels, respectively. Finally, $W = (L-b)$ and $a = ((m-b)-(n-1)b)/n$, with $n$ representing the number of coiled-up channels. This will always be an odd number because the proposed model is symmetrical.

The exact impedance of the panel with a slit-type micro-perforation together with the resistive and reactive correction terms (Dah-You, 2000; Cobo *et al.*, 2020; Almeida *et al.*, 2021b) is determined by Eq. 3

$$Z_p = \frac{j\omega\rho_o t}{\Theta}\left[1 - \frac{\tanh(\ni\sqrt{j})}{\ni\sqrt{j}}\right]^{-1} + \frac{\sqrt{2\rho_o\eta\omega}}{2\Theta} + j\omega\rho_o\frac{d_f F_e}{2F(\epsilon)\Theta}, \tag{3}$$

being $\ni = d_f\sqrt{\rho_0\omega/4\eta}$ the perforation constant (Maa, 1998), withal $\omega = 2\pi f$ and $\eta = 1.8134 \times 10^{-5}$ Pa·s representing the angular frequency and viscosity of air, respectively. $\Theta$ is the porosity or filling fraction of the micro slit embedded in the panel, $F(\epsilon) = [1 - 1.4\epsilon + 0.338\epsilon^3 + 0.0679\epsilon^5]^{-1}$is the Fok correction function due the interaction of radiation of the

air when cells of the absorber are coupled (Cobo *et al.*, 2020), $\epsilon = d_f/L$ and $F_e$ denotes the complete elliptic integral in which an appropriately shaped ellipse approaches the slit, which is abtained by Eq. 4 (Dah-You, 2000)

$$F_e = \int_0^{\frac{\pi}{2}} \frac{d\theta}{\sqrt{1 - e^2 \sin^2 \theta}}, \tag{4}$$

where $e = \sqrt{1 - (d_f/2L_f)^2}$ is the eccentricity of the ellipse. The acoustic impedance of the each coiled-up channel is obtained by

$$Z_{e_1} = Z_{e_2} = -j\sqrt{\frac{\rho_{eq}}{C_{eq}}} \cot\left(\omega\sqrt{\rho_{eq}C_{eq}}L_{eff}\right), \tag{5}$$

$L_{eff} \approx ((n-1)(\sqrt{h^2+a^2})/2 + h + \psi)$ being the effective length of propagation and $\psi \approx 12$ mm is an average factor for correction of the effective length of propagation. $\rho_{eq}$ and $C_{eq}$ are the complex density and compressibility functions, correspondingly, both derived from the visco-thermal acoustic theory (Stinson, 1991).

## 3. Numerical simulation by FEM

Numerical simulations using the finite element method were conducted using COMSOL Multiphysics software. A virtual experiment of a rectangular cross-section impedance tube with the interaction between the Acoustics-Thermoviscous modules is adopted in the simulations (see Figure 2). All tube walls are considered rigid (non-slip condition) and isothermal. A sound pressure source of 1 Pa is introduced and placed at the end of the virtual impedance tube and the AMM absorber located at the opposite end. The pressure and velocity responses at two distinct points are recorded to obtain the acoustic impedance ($Z_i = P_i/(v_i Z_0)$) and the sound absorption coefficient ($\alpha_i = 1 - |Z_i - 1/Z_i + 1|^2$), with $i$ being the points 1 and 2. The governing equations of the numerical process include the linearized Navier-Stokes equation, the energy equation, the equation of continuity, and the equation of state for an ideal gas (Beltman, 1999).

$$\begin{aligned}
&\rho_0 \tfrac{\partial \mathbf{v}}{\partial t} = -\nabla P + \left(\tfrac{4}{3}\eta + \mu_B\right)\nabla(\nabla \cdot \mathbf{v}) - \eta\nabla \times (\nabla \times \mathbf{v}),\\
&\rho_0 C_p \tfrac{\partial T}{\partial t} = \tfrac{\partial P}{\partial t} + \kappa\nabla(\nabla T),\\
&\tfrac{\partial \rho}{\partial t} = -\rho_0 \nabla \cdot \mathbf{v},\\
&P = \rho R_0 T,
\end{aligned} \tag{6}$$

where $\mathbf{v}$, $\rho$, $P$, $T$, $\mu_B$, $\kappa$, $C_p$ and $R_0$ represent, respectively, the velocity vector, air density, pressure, temperature, bulk viscosity ($1.21 \times 10^{-5}$ Pa·s), thermal conductivity, heat capacity at constant pressure (1007 J·kg$^{-1}$·K$^{-1}$) and gas constant (8.32 J·mol$^{-1}$·K$^{-1}$).

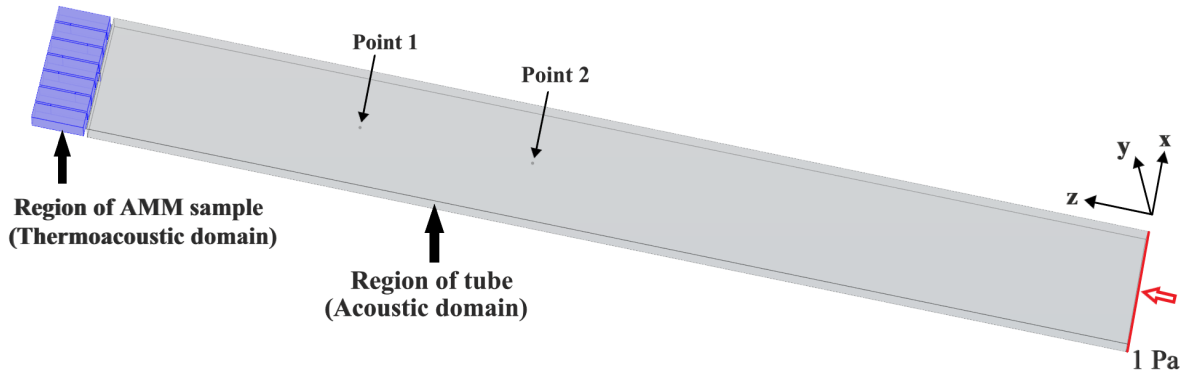


Figure 2. Impedance tube virtual test arrangement.

## 4. RESULTS AND DISCUSSIONS

In this section, we present the results of the AMM behavior. Initially, the theoretical and numerical results are shown with a discussion about the mechanism underlying its performance. Finally, an experimental validation of the sound absorption of AMM is presented.

### 4.1 Theoretical and numerical behavior of the AMM

The behavior of the absorber was performed with the implementation of the sound absorption coefficient and the surface impedance of different unit cells, some cells are illustrated in Fig. 3. The geometric parameters used in the analyzes are shown in Tab. 1. The value of the elliptic integral ($F_e$) is 4.0 (meaning that the slit used to approach the ellipse has a very high proportion largest to the smallest parameter) and the correction due to the interaction of the air radiation in the panel slit ($F(\epsilon)$) is 1, since the panel presents only one perforation, and, therefore, there is no interaction between perforations.

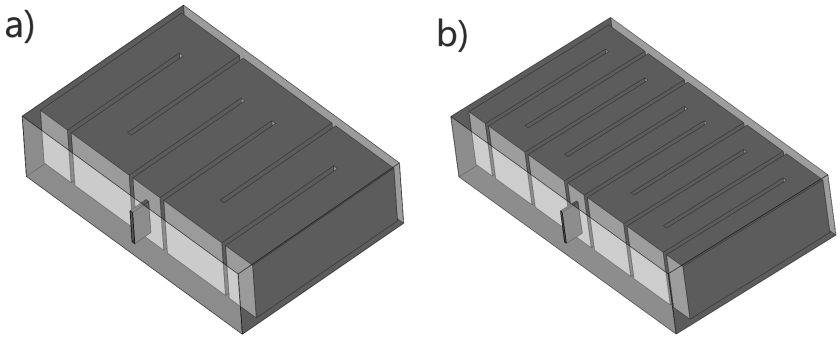


Figure 3. Configurations of the symmetrical labyrinth metamaterial. a) with 7 and b) 11 coiled-up channels, respectively.

Table 1. Parameters used and calculated in the analysis of individual cells. (Unit: mm)

| Geometrical parameters | $d_f$ | $L_f$ | $m$ | $h$ | $b$ | $L$ | $t$ |
|---|---|---|---|---|---|---|---|
| Value | 0.36 | 9.0 | 46.0 | 26.0 | 1.0 | 13.0 | 1.0 |

| Calculated parameters | n = 5 | n = 7 | n = 9 | n = 11 |
|---|---|---|---|---|
| $a$ (space cross-sectional width) | 8.20 | 5.57 | 4.11 | 3.18 |
| $L_{eff}$ (effective propagation length) | 88.5 | 113.7 | 139.3 | 165.0 |

Figure 4 shows the theoretical behavior of the different absorber cells. The sound absorption peaks are located with their respective amplitude at 526 Hz (0.995), 469 Hz (0.990), 410 Hz (0.985) and 363 Hz (0.980) for $n = 5$, 7, 9 and 11 coiled-up channels, respectively. The sound absorption peak moves to low frequencies as $n$ increases. This displacement is due to the increase in the effective propagation length $L_{eff}$ and the greater influence of the visco-thermal effects, the

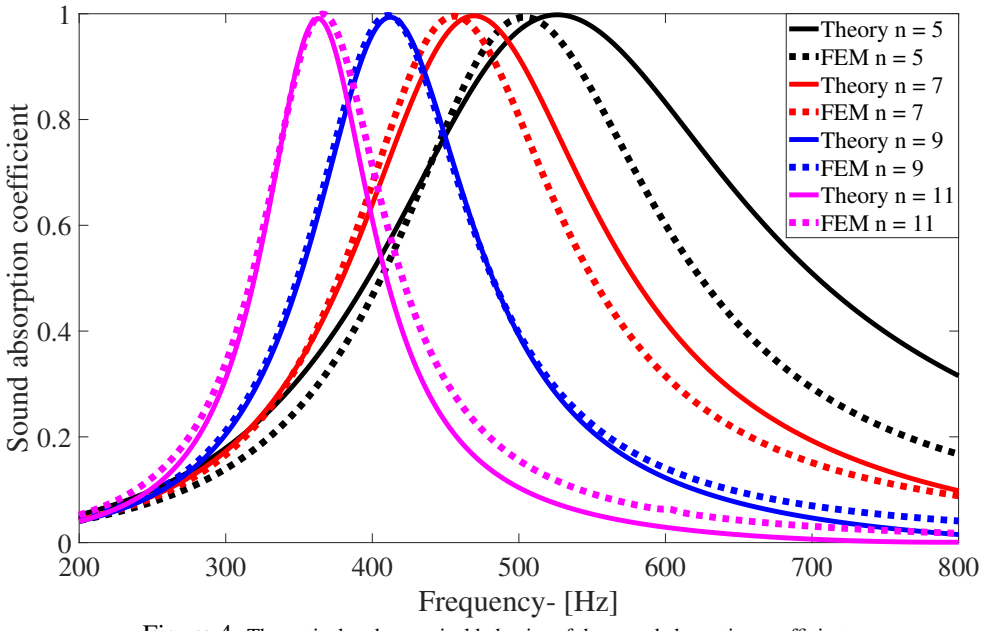


Figure 4. Theoretical and numerical behavior of the sound absorption coefficient.

area decreases with an increasing value of $n$, i.e., $S_i(n = 5) \approx 98.4$ mm$^2$, $S_i(n = 7) \approx 66.9$ mm$^2$, $S_i(n = 9) \approx 49,3$ mm$^2$ and $S_i(n = 11) \approx 38.2$ mm$^2$. The relative bandwidths at 50% of the maximum absorption are 305 Hz, 200 Hz, 132 Hz and 91 Hz for $n = 5$, 7, 9 and 11 coiled-up channels, respectively. Consequently, respective values for the relationship between the bandwidth and the center frequency are 60.0%, 42.6%, 32.2% and 25.0%.

It can be seen in Fig. 4 that the AMM has a broadband absorption, which demonstrates that the concept of double coiled-up channels increases the capacity of the model to absorb a greater amount of sound energy, although this width of bandwidth decreases as $n$ increases. We will discuss below that, although a portion of this energy is proportionally dissipated with the increase of these wound channels, most of this energy is dissipated in the micro slit region of the panel. The numerical validation of the behavior of the model is shown in Fig. 4 and a good agreement between the methods is verified, mainly with the increase of the symmetrical coiled-up channels of the absorber. This greater agreement is due to the greater influence of viscothermal effects because the section area of the channels decreases with increasing $n$. The displacement of the sound absorption peak to lower frequencies is corroborated by the numerical analysis. Such behavior is due to the high level of resonance produced by the strong air compression in the micro slit, leading to a greater viscous dissipation. Moreover, the greatest disagreement between the methods occurs at the bandwidth to 50% of the maximum absorption, whose relative error is 28.5% and at the peak frequency whose error is 5%, both for the model with $n = 5$ coiled-up channels.

The good behavior of the sound absorption coefficient of the AMM is associated with the strong coupling between its surface impedance and the air impedance. The real and imaginary parts of the normalized surface impedance of the absorber are represented in Fig. 5. The real parts are 0.93, 0.89, 0.85 and 0.83 at frequencies 526 Hz, 469 Hz, 410 Hz and 363 Hz, respectively. Meanwhile, the imaginary parts are zero for these same frequencies. Note that total sound absorption is almost achieved when $n = 5$, where the real part is closer to the unit value, demonstrating an acoustic strong coupling between the surface impedance of the absorber and the medium (air).

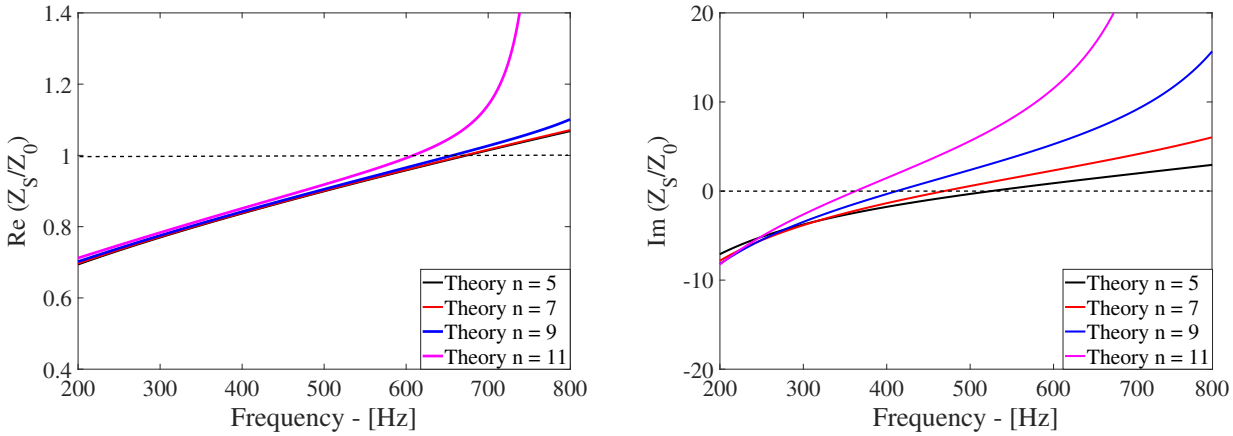


Figure 5. Normalized surface impedance behavior of the model.

To explore the low frequency absorption mechanism of AMM, the acoustic pressure field at the resonance frequency for two cells with $n = 5$ and 9 coiled-up channels are mapped in Fig. 6 a) and b), respectively. It is observed that in both cases, the sound pressure at the end of the symmetrical coiled-up channels is four and seven times greater than at the entrance of the micro slit of the panel.

The mechanism underlying the sound absorption performance of the AMM was also explored through comparisons

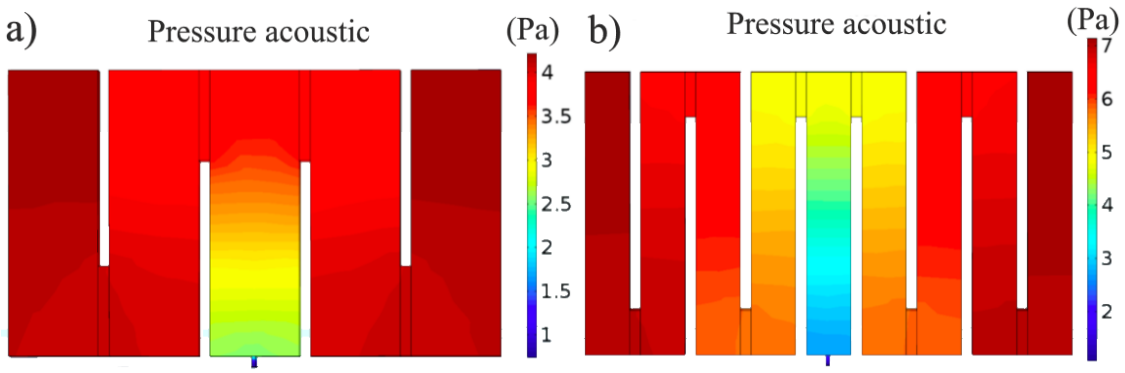


Figure 6. a) - b) Sound pressure field of the cells with $n = 5$ and 9 coiled-up channels at the operating frequencies of 504 Hz and 410 Hz, respectively.

between the different types of sound energy dissipation in cells with $n = 5$ and 9 symmetrical coiled-up channels. Fig. 7 illustrates the behavior of these two types of dissipation, in which there is a predominance of viscous dissipation that occurs mainly in the micro slit of the panel. On the other hand, thermal dissipation is much lower compared to the viscous dissipation and is distributed at the end of the micro slit and on the surface of the inner walls and curvatures of the coiled-up channels. In statistical terms, we observed that the thermal energy dissipation represents 0.010% (for $n = 5$) and 0.014% (for $n = 9$). In other words, the finding that approximately 99.9% of the maximum energy dissipation in both cases is of the viscous type and that it occurs primarily in small areas (micro slit) justifies the physical mechanism of sound absorption of the AMM, since the micro slit coupled to the symmetrical coiled-up channels constitutes a Helmholtz resonator. Furthermore, when the sound frequency approaches the resonant frequency of the cell (410 Hz for $n = 9$), the air in the narrow areas oscillates severely. Thus, the friction between the air and the inner wall of the micro slit significantly dissipates the energy of the sound wave (see Fig. 7 e) ), thus causing a great loss of energy in that region (Li *et al.*, 2018; Tang *et al.*, 2017a) .

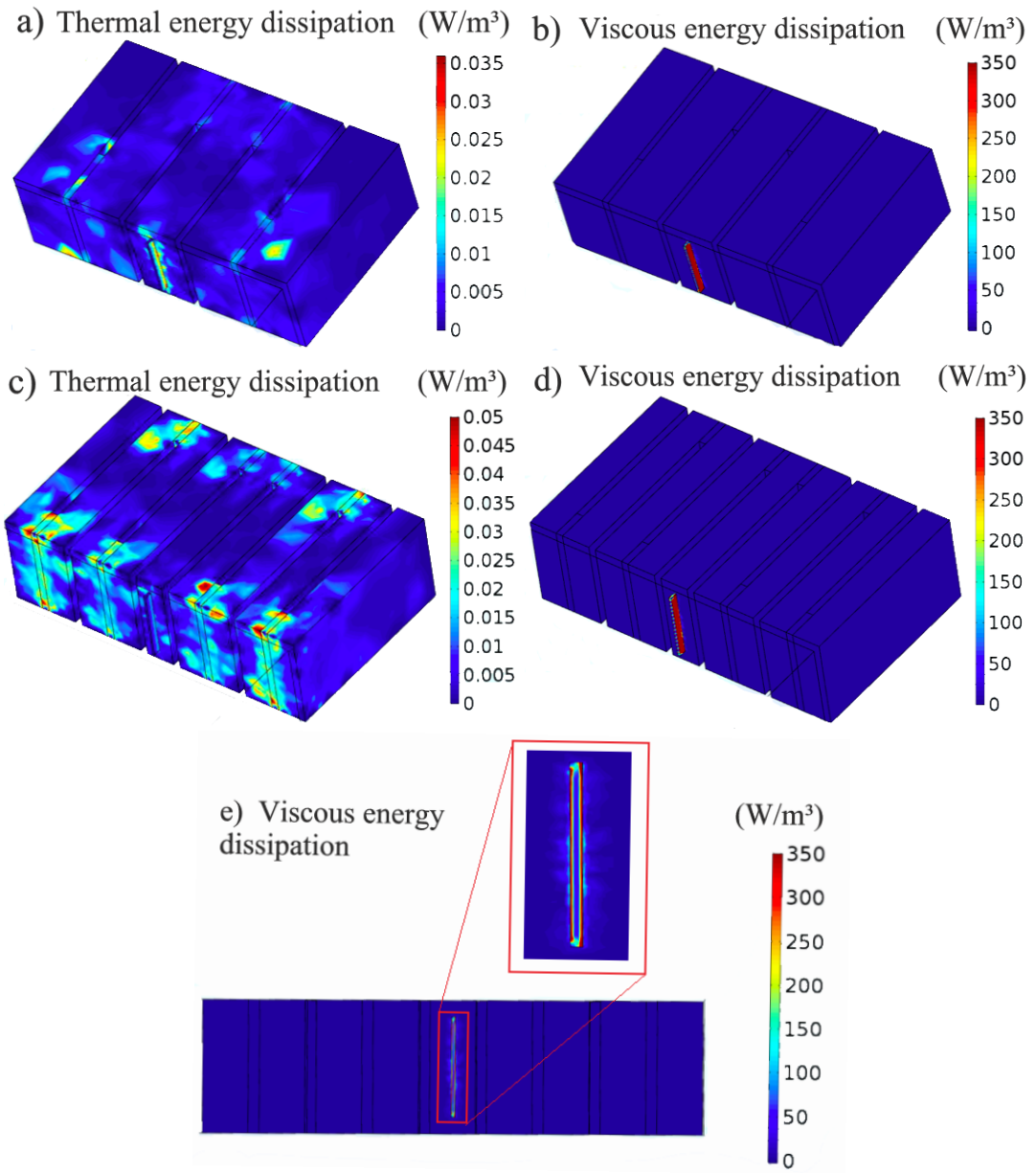


Figure 7. 3D contour of the energy dissipation in the sectional plane of a cell with $n = 5$ and 9 symmetrical coiled-up channels at the operating frequency 504 Hz and 410 Hz, respectively.

### 4.2 Experimental results

The sound absorption coefficient performance of an AMM sample was assessed for a 107 mm diameter cylindrical impedance tube, corresponding to a plane wave cutoff frequency of $\approx$ 1877 Hz. The sample is composed of eight composite unit cells of $n = 5$ symmetrical coiled-up channels. The geometric parameters used are listed in Tab. 2. The experimental setup is illustrated in Fig. 8 a), note that we used the standard two-microphone method (Din, 2001) to measure the sound absorption coefficient, which makes this practice consistent with the numerical simulations performed. Fig. 8 b) and c) illustrate a sketch and the sample manufactured through a cartesian printer by means of the extrusion technique of material from additive manufacturing using ABS (acrylonitrile butadiene styrene) as raw material.

Table 2. Parameters used in the manufacture of sample. (Unit: mm)

| Geometrical parameters | $d_f$ | $L_f$ | $m$ | $h$ | $b$ | $L$ | $t$ |
|---|---|---|---|---|---|---|---|
| Value | 0.56 | 7.0 | 58.0 | 40.0 | 1.0 | 14.5 | 4.0 |

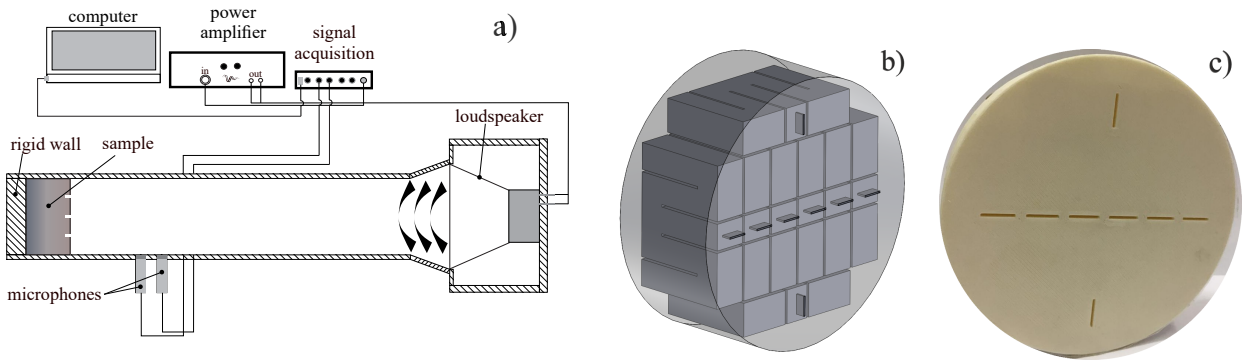


Figure 8. a) Schematic diagram of the impedance tube system, b) Sketch of the structure and c) printout of sample containing 8 cells with $n = 5$ coiled-up channels for the experiment.

Figure 9 compares the results of the theoretical, numerical and experimental sound absorption coefficient for the absorber and a summary of the main results is presented in Tab. 3, where a good agreement is achieved between the results both in the frequency and amplitude. The match between the theory and experimental methods is corroborated by the strong coupling of the acoustic impedance, the real and imaginary parts of the absorber surface impedance normalized by the air impedance are illustrated in Fig. 10. It is important to highlight at low frequency the absolute value of Im($Z_S$) is greater than that of Re($Z_S$), so that the frequency of the peak absorption is usually determined by the zero of the imaginary part and its amplitude by the real part.

Table 3. Comparison of experimental, numerical and theoretical results for the AMM.

| Method | Peak absorption frequency (Hz) | Peak absorption amplitude | Bandwidth at 50 % (Hz) |
|---|---|---|---|
| Theory | 243 | 0.99 | 117 |
| Numerical | 235 | 0.99 | 98 |
| Experimental | 242 | 0.97 | 158 |

It can also be seen by the Figure 9 that the corresponding values of the relationship between the bandwidth and the central frequency are 48.1%, 41.7 % and 65% for the theoretical, numerical and experimental methods, respectively. Moreover, the experimental bandwidth relative to 50% of the maximum absorption is observed to be significantly larger than the one achieved by the theory. This is probaly due to the additional dissipation of sound energy by the rough internal surface of the channels of the manufactured sample (Kandlikar *et al.*, 2005)

## 5. CONCLUSIONS

A low-frequency absorbing acoustic metamaterial was proposed based on a panel with a micro slit type micro-perforation and symmetrical coiled-up channels. Analytical and numerical (FEM) methods demonstrated good agreement for the sound absorption at low frequencies ($\leq$ 600 Hz). The sound energy dissipation mechanism was investigated and it was concluded that the viscous dissipation in the micro slit region predominates in the absorber. The wideband sound absorption due to the symmetrical coiled-up channels was obtained analytically and experimentally confirmed, with the

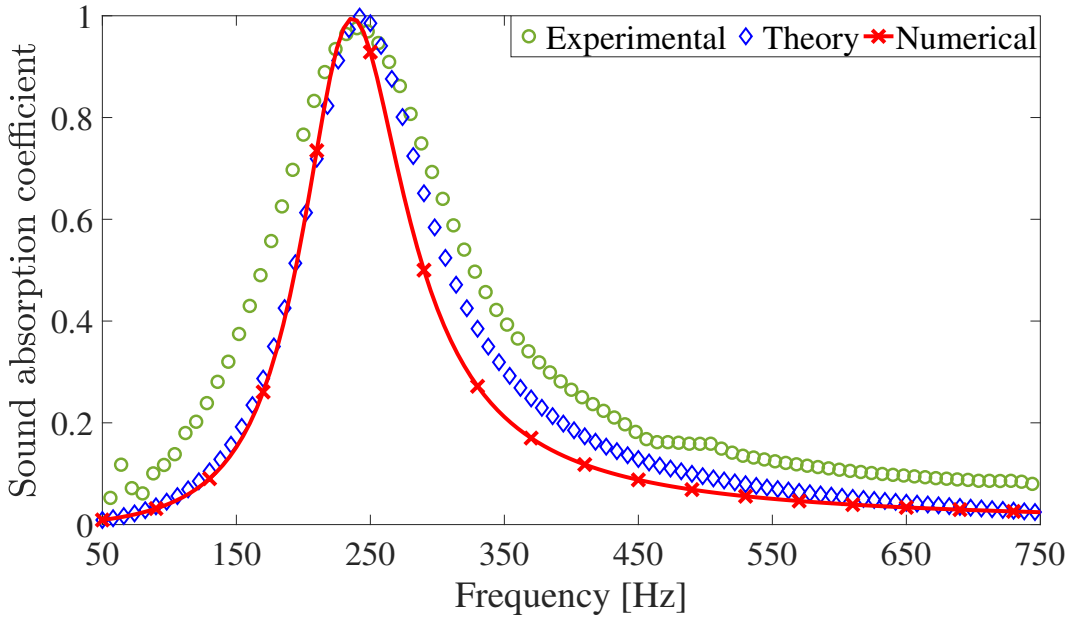


Figure 9. Theoretical, numerical and experimental behavior of the sound absorption coefficient.

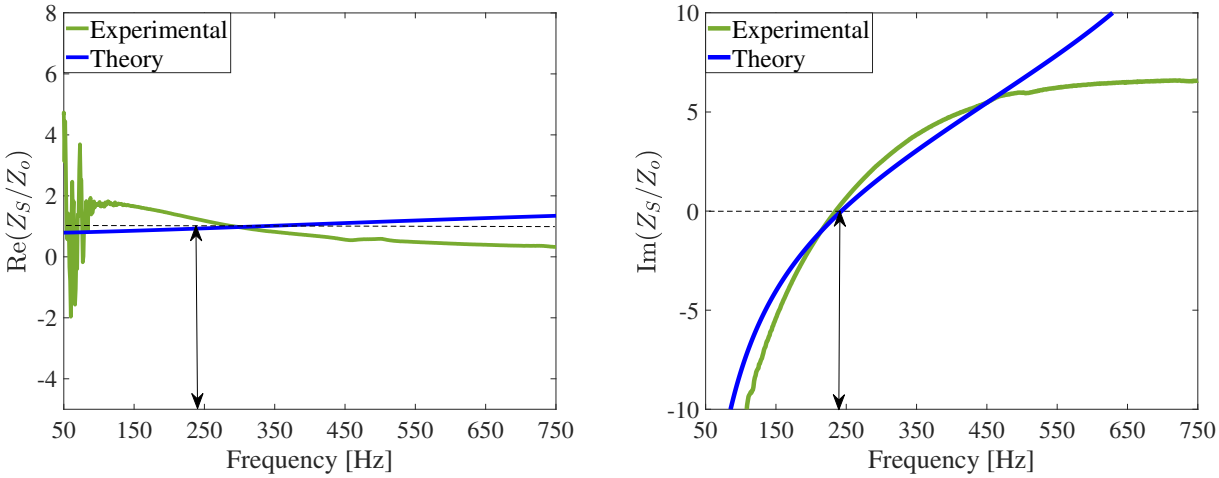


Figure 10. Normalized surface impedance behavior of the model.

absorber showing a sub-wavelength scale, that is, $\lambda/32$. For the case wideband sound absorption greater yet, the coupling in parallel of distinct cells of the absorber is strongly recommended. Finally, the sound absorption performance of the AMM due to its impedance coupling and large energy dissipation makes the absorber an excellent candidate for the control of low frequency sound energy, which is of great interest for engineering noise control.

## 6. ACKNOWLEDGEMENTS

The authors are grateful for the financial support for this research provided by the Graduate Program in Mechanical Engineering (POSMEC) and the Laboratory of Vibrations and Acoustics (LVA) of the Federal University of Santa Catarina.

## 7. REFERENCES

Almeida, G.d.N., Vergara, E.F., Barbosa, L.R., Lenzi, A. and Birch, R.S., 2021a. "Sound absorption metasurface with symmetrical coiled spaces and micro slit of variable depth". *Applied Acoustics*, Vol. 183, p. 108312.

Almeida, G.N., Vergara, E.F., Barbosa, L.R. and Brum, R., 2021b. "Low-frequency sound absorption of a metamaterial with symmetrical-coiled-up spaces". *Applied Acoustics*, Vol. 172, p. 107593.

Almeida, G.N., Vergara, E.F., Barbosa, L.R., Lenzi, A. and Birch, R.S., 2021c. "A low-frequency sound absorber based

on micro-slit and coiled cavity". *Journal of the Brazilian Society of Mechanical Sciences and Engineering*, Vol. 43, No. 3.

Beltman, W., 1999. "Viscothermal wave propagation including acousto-elastic interaction, Part I : Theory". *Journal of Sound and Vibration*, Vol. 227, No. 3, pp. 555–586.

Cai, X., Guo, Q., Hu, G. and Yang, J., 2014. "Ultrathin low-frequency sound absorbing panels based on coplanar spiral tubes or coplanar helmholtz resonators". *Applied Physics Letters*, Vol. 105, No. 12, p. 121901.

Carvalho de Sousa, A., Deckers, E., Claeys, C. and Desmet, W., 2021. "On the assembly of archimedean spiral cavities for sound absorption applications: Design, optimization and experimental validation". *Mechanical Systems and Signal Processing*, Vol. 147, p. 107102.

Cobo, P., de la Colina, C. and Simón, F., 2020. "On the modelling of microslit panel absorbers". Vol. 159, p. 107118.

Dah-You, M., 2000. "Theory of microslit absorbers". *Acta Acustica*, Vol. 25, No. 6, pp. 481–485.

Din, E., 2001. "10534-2: Acoustics-determination of sound absorption coefficient and impedance in impedance tubes-part 2: Transfer-function method".

Gan, W.S., 2018. *New Acoustics Based on Metamaterials, Springer Singapore*.

Kandlikar, S.G., Schmitt, D., Carrano, A.L. and Taylor, J.B., 2005. "Characterization of surface roughness effects on pressure drop in single-phase flow in minichannels". *Physics of Fluids*, Vol. 17, No. 10, p. 100606.

Langfeldt, F., Kemsies, H., Gleine, W. and von Estorff, O., 2017. "Perforated membrane-type acoustic metamaterials". *Physics Letters A*, Vol. 381, No. 16, pp. 1457–1462.

Leblanc, A. and Lavie, A., 2017. "Three-dimensional-printed membrane-type acoustic metamaterial for low frequency sound attenuation". *The Journal of the Acoustical Society of America*, Vol. 141, No. 6, pp. EL538–EL542.

Li, J., Wang, W., Xie, Y., Popa, B.I. and Cummer, S.A., 2016. "A sound absorbing metasurface with coupled resonators". *Applied Physics Letters*, Vol. 109, No. 9, p. 091908.

Li, L., Gang, X., Liu, Y., Zhang, X. and Zhang, F., 2018. "Numerical simulations and experiments on thermal viscous power dissipation of perforated plates". *AIP Advances*, Vol. 8, No. 10, p. 105221.

Long, H., Shao, C., Liu, C., Cheng, Y. and Liu, X., 2019. "Broadband near-perfect absorption of low-frequency sound by subwavelength metasurface". *Applied Physics Letters*, Vol. 115, No. 10, p. 103503.

Maa, D.Y., 1998. "Potential of microperforated panel absorber". *The Journal of the Acoustical Society of America*, Vol. 104, No. 5, pp. 2861–2866.

Stinson, M.R., 1991. "The propagation of plane sound waves in narrow and wide circular tubes, and generalization to uniform tubes of arbitrary cross-sectional shape". Vol. 89, No. 2, pp. 550–558.

Tang, Y., Ren, S., Meng, H., Xin, F., Huang, L., Chen, T., Zhang, C. and Lu, T.J., 2017a. "Hybrid acoustic metamaterial as super absorber for broadband low-frequency sound". *Scientific Reports*, Vol. 7, No. 1.

Tang, Y., Xin, F., Huang, L. and Lu, T., 2017b. "Deep subwavelength acoustic metamaterial for low-frequency sound absorption". *EPL (Europhysics Letters)*, Vol. 118, No. 4, p. 44002.

Wu, X., Fu, C., Li, X., Meng, Y., Gao, Y., Tian, J., Wang, L., Huang, Y., Yang, Z. and Wen, W., 2016. "Low-frequency tunable acoustic absorber based on split tube resonators". *Applied Physics Letters*, Vol. 109, No. 4, p. 043501.

Zhao, X., Cai, L., Yu, D., Lu, Z. and Wen, J., 2017. "A low frequency acoustic insulator by using the acoustic metasurface to a helmholtz resonator". *AIP Advances*, Vol. 7, No. 6, p. 065211.